Partanen, Lauri; Hakala, Mikko; Laasonen, Kari

Hydrogen adsorption trends on various metal-doped Ni_2P surfaces for optimal catalyst design

Hydrogen adsorption trends on various metal-doped Ni_2P surfaces for optimal catalyst design

Lauri Partanen, Mikko Hakala, and Kari Laasonen[*]

Department of Chemistry and Materials Science, Aalto University, P.O. Box 16100, FI-00076 Aalto, Finland

E-mail: kari.laasonen@aalto.fi

Abstract

In this study, we looked at the hydrogen evolution reaction on Mg-, Mo-, Fe-, Co-, V-, and Cu-doped Ni_3P_2 and Ni_3P_2+P terminated Ni_2P surfaces. The DFT calculated hydrogen adsorption free energy was employed as a predictor of the materials' catalytic HER activity. Our results indicate that doping can substantially improve the catalytic activity of the Ni_3P_2 terminated surface. In contrast, the Ni_3P_2+P terminated one seems to be catalytically active irrespective of the type of doping, including in the absence of doping. Based on our doping energy and adsorption free energy calculations, the most promising dopants are iron and cobalt, whereas copper is less likely to function well as a doping element.

1 Introduction

Due to the broad-ranging detrimental climate effects associated with the burning of fossil fuels, the impending rise in the global population, and the consequent increase in energy

demand, the development of cleaner energy sources has become a top priority within the scientific community.[1–3] However, the intermittent nature of solar and wind energies means that an efficient storage system is required to realise their potential.[1,2] The absence of carbon emissions during conversion, high energy density, long-term storage capability, and flexibility of use both in mobile and stationary applications make hydrogen an appealing energy depository.[4] One of the most promising candidates for large-scale hydrogen production is water-splitting through electrolysis, which enables the clean conversion of water into hydrogen and oxygen gases.[3,5]

The hydrogen evolution reaction (HER) occurs at the cathode of a water-splitting cell, while the four-electron oxygen evolution reaction (OER) takes place at the anode. Hydrogen production through reduction (i.e., $H^+(aq) + e^- \rightarrow \frac{1}{2}H_2(g)$) is a two-step process where two alternative reaction pathways are typically considered.[6] Both pathways start with the Volmer reaction, where hydrogen adsorbs on a surface site symbolised by an asterisk *:

$$H^+(aq) + e^- + {}^* \rightarrow {}^* H. \tag{1}$$

This is followed either by the Tafel reaction, where two surface-adsorbed hydrogens join together

$$^*H + {}^*H \rightarrow H_2(g) + 2\ {}^*, \tag{2}$$
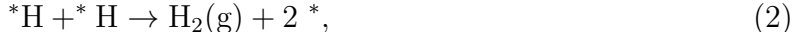
or by the Heyrovsky reaction, where the second proton arrives directly from the solution

$$^*H + H^+(aq) + e^- \rightarrow H_2(g) + {}^* . \tag{3}$$
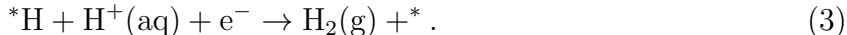
Reactions (1), (2), and (3) summarise HER in acidic solutions.

Irrespective of the exact reaction mechanism, efficient catalysts are mandatory for turning the dream of a hydrogen energy economy into reality. While noble metals like Pt are some of the best HER catalysts, their high cost and scarcity hinder large-scale application.[3] Thus, recent studies have looked at HER on various non-precious materials like heteroatom-doped

nano-carbons,[7–10] together with nitrides, oxides, carbides, selenides, and sulfides of transition metals,[7] which could replace platinum as the principal HER catalysts.

Compared to the other transition metal compounds, phosphides like MoP, CoP, and Ni_2P display HER activities on par with the best transition metal catalyst like MoS_2.[7,11–13] Generally speaking, phosphides possess advantages either in terms of synthesis routes or catalytic performance over the other classes of transition metal compounds. For example, MoS_2 needs to be nanostructured into nanosheets to yield catalytic properties comparable to MoP,[7,14] which can show high HER ability even in its bulk state.[15] Particularly, nickel phosphide nanostructures like nanosheets and -particles have emerged as promising materials for HER catalysis under acidic conditions.[7,11,12,16–18]

Chemical doping provides a novel way of enhancing the catalytic activity of many of the non-noble metal catalysts.[7] In the case of Ni_2P, transition metal dopants such as Mo,[19] Al,[20] Mn,[21] W,[22] and Fe[23,24] have been experimentally demonstrated to improve the HER activity. On the computational side, in our previous density functional theory (DFT) study of transition metal doping of a MoS_2 surface, we showed that the H-adsorption strength in the Volmer step depends on the microscopic structure of the surface and the nature of the dopant.[25] A similar result regarding the microscopic nature of the surface was observed in our computational study of aluminium doping on Ni_2P.[26]

In this article, we expand our previous investigation of the impact of Al doping on the HER activity of Ni_2P[26] to include the dopants Mg, Mo, Fe, Co, V and Cu. As before, we focus on the two most stable Ni_2P surface terminations: Ni_3P_2 and phosphorised Ni_3P_2+P.[27,28] We utilise the typical hydrogen adsorption free energy (ΔG_H) approach for HER activity, which has also been employed in previous Ni–P studies.[26,29] In this approach, ΔG_H on the electrode surface is used as a descriptor for predicting the catalytic activity with respect to a molecular $H_2(g)$ reference.[6] In line with Sabatier's principle, a value $\Delta G_H \approx 0$ indicates that the hydrogen neither binds too weakly nor too strongly to the surface, and corresponds to good HER activity.[30] As, for example, the choice of DFT functional affects the ΔG_H

3

values,[26] following Greeley et al.[30] we consider sites with $|\Delta G_{\mathrm{H}}| < 0.1$ eV as optimal. Our primary goal is to understand how different dopants and doping induced surface structures impact HER activity and to suggest doping schemes that result in improved catalysts.

2   Systems and methods

2.1   Computational details

All our DFT calculations utilised the QUICKSTEP module[31] of the publicly available CP2K simulation suite.[32] The package employs the hybrid Gaussian/plane wave method where the wave functions are represented in a Gaussian-type basis and an auxiliary plane-wave basis is used for the electronic density. As in our previous Ni_2P and MoS_2 studies,[25,26] the Perdew–Burke–Ernzerhof (PBE) functional[33] was used with the Kohn–Sham orbitals expanded in the molecularly-optimised double-valence polarised basis set (MOLOPT-SR-DZVP) and the core electrons represented by the Goedecker–Teter–Hutter pseudopotentials (GTH).[34–36] In all calculations, the plane-wave kinetic energy cut-off was set to 700 Ry and the cutoff for the reference grid to 60 Ry. The force convergence criterion of the geometry optimisations was left to its default value of 0.023 eV/Å. The Poisson equation for the electrostatic potential was solved with periodic boundary conditions.

The Ni_2P bulk lattice parameters were taken from our previous study,[26] where a supercell of $4 \times 4 \times 4$ unit cells was allowed to relax under a 0.1 kbar pressure tolerance. The system relaxed to a nonferromagnetic state with cell parameters $a = b = 5.860$ Å and $c = 3.332$ Å. For the calculation of the atomic reference energies of Ni, Mg, Mo, Fe, Co, Cu, and V in the crystalline phase, we employed a supercell of $10 \times 10 \times 10$ units with the PBE lattice parameters taken from the literature.[37–40] Our original Ni_2P calculation employed the orbital transformation method, whereas in the reference energy calculation the diagonalisation method was used with the Fermi temperature set to 75 K. The effect of increasing this temperature to 300 and 400 K was studied but the impact on the energy/atom was less than

0.02 eV in all cases.

Our surface calculations used the same diagonalisation method with a 75 K electronic smearing but included the Grimme D3(BJ) dispersion corrections.[41,42] Of the different surface structures for Ni_2P, we focused on the Ni_3P_2 termination of the (0001) surface because it is the preferred bulk-like termination in the Ni_2P stability region.[27,43] At around pH=0, which corresponds to the typical experimental conditions for HER in acid, this surface phase dominates at potentials $U > -0.21$ V vs. the standard hydrogen electrode.[28] Below this region, there is both experimental and computational evidence that the surface becomes enriched by phosphorus.[27,28,44–49] Specifically, the Ni_3P_2+P termination predominates within the potential region -0.21 V $\geq U \geq -0.36$ V, whereas below this range the pristine Ni_3P_2 surface becomes passivated by H atoms on the Ni_3 hollow sites.[28] Hence, both Ni_3P_2 and Ni_3P_2+P surfaces were included in this study.

Based on our previous hydrogen adsorption free energy test calculations on 5, 7, 9, 11, and 13 layer slabs,[26] we modelled our two surfaces with a seven layers deep symmetric slab where the atoms at the bottom layer were fixed to their bulk positions. At least a 10 Å wide vacuum layer was used on both sides of the slab. For Ni_3P_2+P, the extra phosphorus atom was added to the Ni_3 hollow site of the Ni_3P_2 structure, as depicted in Figure 1. In both cases, $5 \times 5 \times 1$ Monkhorst-Pack **k**-points were utilised.

2.2 HER activity model

Our analysis of the H-coverage and differential Gibbs free energies of the H-adsorption followed the self-consistent scheme proposed by Nørskov et al.[6] and Skúlason et al.[50] According to this scheme, the relevant H coverage at a particular chemical potential μ is determined by the minimum of the total adsorption energy $\Delta_{tot}G_H(n)$:

$$\Delta_{tot}G(n) = G(n) - G(0) - n\mu \tag{4}$$

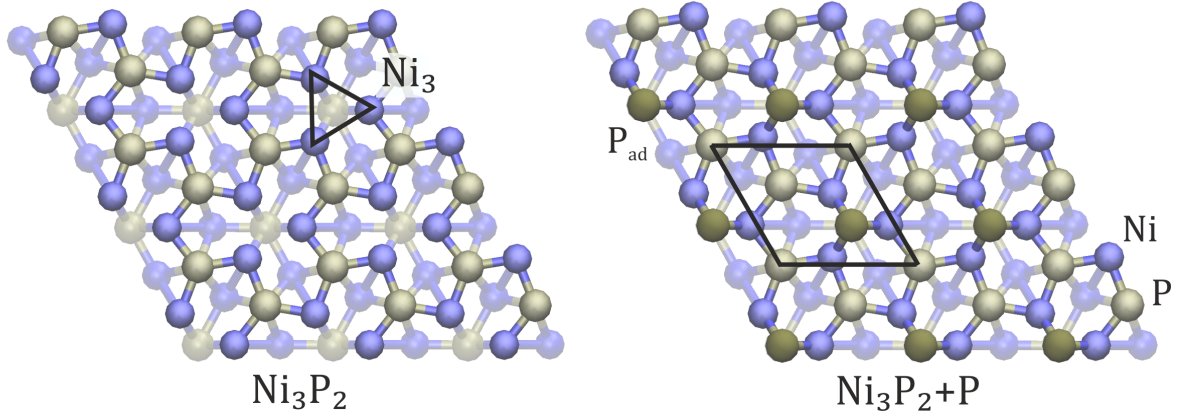Figure 1: A surface representation of the Ni_3P_2 and Ni_3P_2+P terminations of Ni_2P. In this and all remaining figures, the hydrogen atoms are indicated by white, the phosphorus atoms by yellow-brown, the Ni atoms by deep blue, and the metal atoms by teal. The pshophorus adatom is marked by P_{ad}.

where $G(n)$ is the free energy of the surface with n hydrogen atoms attached and $G(0)$ is the free energy of the bare surface. The chemical potential of hydrogen is given by[29]

$$\mu = \frac{1}{2}G(H_2) - eU \tag{5}$$

where $G(H_2)$ is the free energy of molecular hydrogen in the gas phase and U is the cathode potential. For comparison of different adsorption sites, the differential Gibbs free energy of adsorption

$$\Delta G_H(n) = G(n) - G(n-1) - \mu, \tag{6}$$

plays a crucial role. By using a factor of 0.24 eV to account for all the differences in entropic and zero-point energy contributions between the products and reactants at pH=0,[6,29,51] this equation simplifies into

$$\Delta G_H(n) = E(n) - E(n-1) - \frac{1}{2}E(H_2) + 0.24 \text{ eV} + eU \tag{7}$$

where $E(n)$ is the total energy at 0 K with n hydrogen atoms attached to the surface. It is directly obtained from DFT calculations. The minimum overpotential to adsorb hydrogen at a given H coverage n is

$$\eta(n) = \frac{\min \Delta G_{\mathrm{H}}(n)}{e} \tag{8}$$

where the minimum is taken over the different surface sites studied. In our calculations, we used a set of 14 initial positions for the hydrogen above the slab. Because our previous test calculations for charged pristine and Al-doped surfaces failed to show any charge trapping,[26] we consider only the neutral states in this article, i.e., where $U = 0$ V.

3   Results and discussion

As illustrated in Figure 2, the Ni_3P_2 terminated Ni_2P surface has alternating Ni_3P_2 and Ni_3P layers.[52,53] The dopant atoms were restricted to the top four layers. To identify the different doping schemes, the notation lxdy is used where x is the layer of the dopant atoms (i.e. $x \in \{1, 2, 3, 4\}$) and y is their number (i.e. $y \in \{1, 2, 3\}$). In cases where dopants were present in two layers, we employ the simpler notation lx_1lx_2, where x_1 and x_2 tell the layers of the two dopant atoms, respectively, since we only investigated cases with one dopant atom per layer.

3.1   Doping energies

Ni_3P_2 termination

The doping energies for the Ni_3P_2 termination of Ni_2P are shown in Figure 3. As can be seen, regardless of layer, most metals show a linear trend as the number of dopants in the layer increases. For Co this trend is always strongly negative, implying that thermodynamically the lattice structure is very susceptible to cobalt doping, due to it's high reactivity and comparable size to Ni. In contrast, the doping energy is always positive for the less reactive
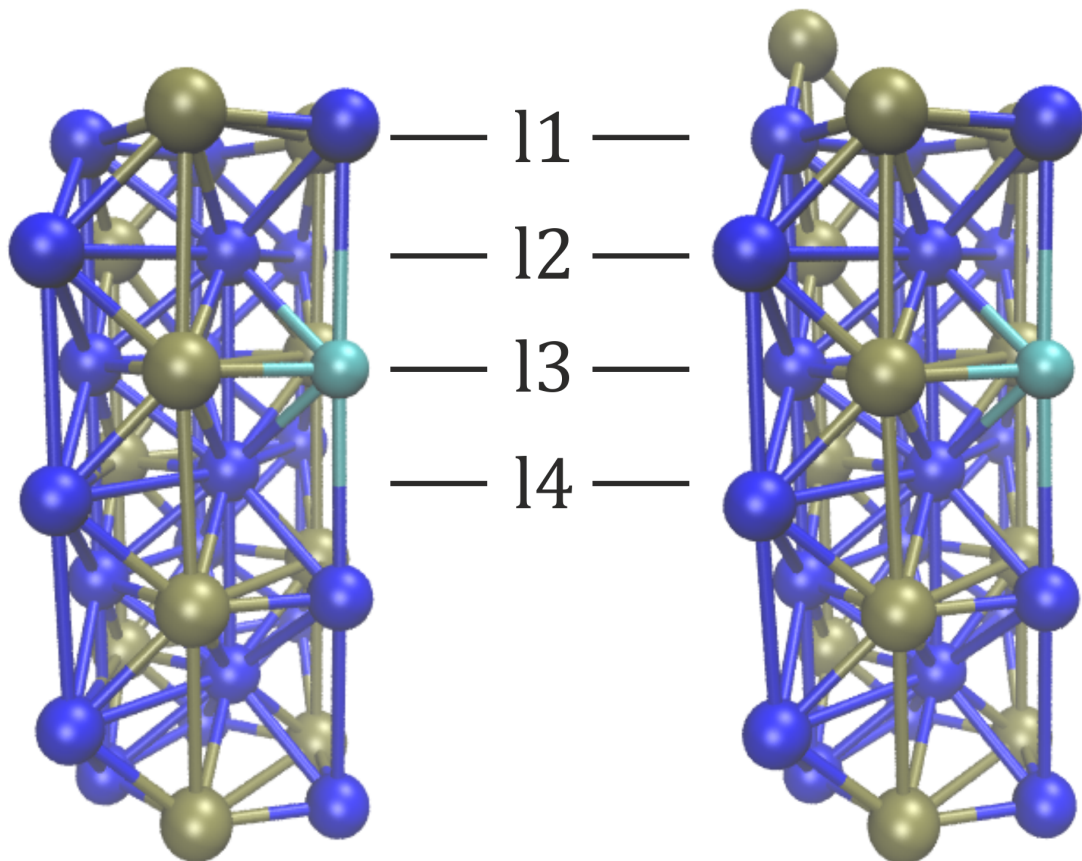
Figure 2: The slab model for the Ni_3P_2 and Ni_3P_2+P terminated Ni_2P surface. In the Figure, the third layer is doped by a single metal atom which corresponds to an l3d1 doping scheme.

Cu. For other dopants, the sign and steepness of the slope depend on the layer. For V and Mo, the doping energies are positive or near zero and generally increase with increasing number of dopants for the 1st and 3rd layers, and negative and decreasing for the 2nd and 4th layers. In contrast, for iron, the doping energies are positive and increasing only for the first layer and then negative and decreasing for the other three.

The large deviations from linear behaviour for Mo and Mg in the third layer are accompanied by radical surface reconstructions. For example, in the double and triple doping for Mg and the triple doping in Mo, one of the P atoms moves away from the third Ni_3P_2 layer, creating a vacancy and a surface structure that resembles the Ni_3P_2+P one. In most cases, the introduction of dopants causes no substantial changes in geometry. For Fe and Co, it results in a slight contraction of the slab with the magnitude generally depending on the number of dopants, and for the other metals a slight expansion. Interestingly, for first layer Mg doping, the Mg atoms lift up from the surface, staying more than 0.6 Å above the corresponding Ni atoms. Similarly, for the triple Mo doping of the first layer, the atoms of the two topmost layers of the Ni_2P surface lift up from the surface, while the P atom from the first layer moves down to the second one.

Ni_3P_2+P termination

The doping energies for the Ni_3P_2+P termination are shown in Figure 4. As in Figure 3, most energies behave linearly with respect to increasing number of dopant atoms within a given layer. The clearest trends are observed for Cu and Co. In the case of Cu the formation energy of the doped lattice is always positive and increases with the number of dopant atoms. For Co, the energies are always strongly negative and decrease with the number of dopants. As before, in some cases like l3d3 for Mo, significant deviation from linear behaviour is observed due to radical restructuring of the surface.

Comparing the linear trends of different dopants in Figures 3 and 4, one sees that for Mo, V, Co, and Fe the doping energies are higher for the first layer for Ni_3P_2 termination

9

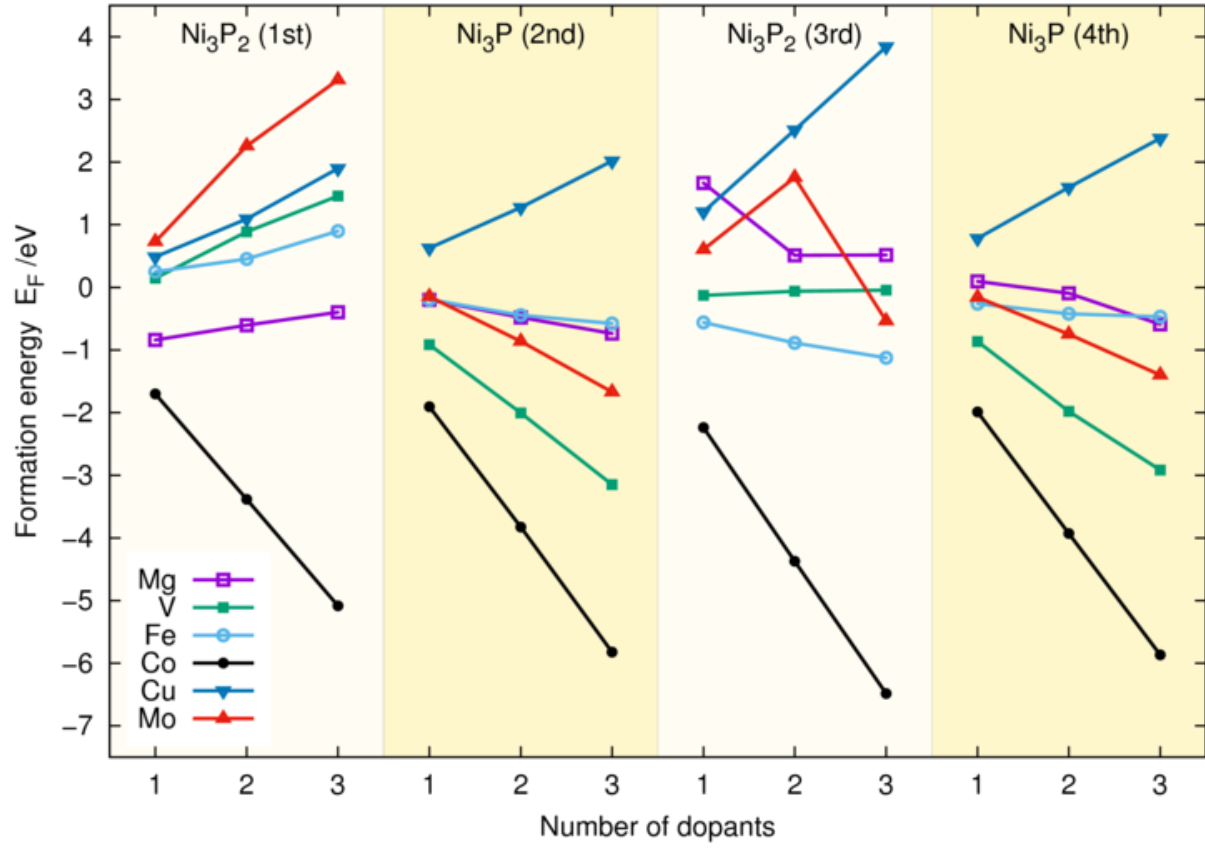Figure 3: Doping energies (E_F) for Mg, V, Fe, Co, Cu, and Mo for the four topmost layers of the Ni_3P_2 termination of Ni_2P.

whereas for Cu, and Mg the energies are lower. Unsurprisingly, in the lower layers, the doping energies are similar. Based on the Figures, we predict that Ni_2P should be readily dopable by Co, Fe, V, Mg, and Mo. In contrast, for Cu, the doping is clearly energetically unfavourable in all cases, and according to our test calculations inserting two Cu atoms to different layers does not remedy the situation.
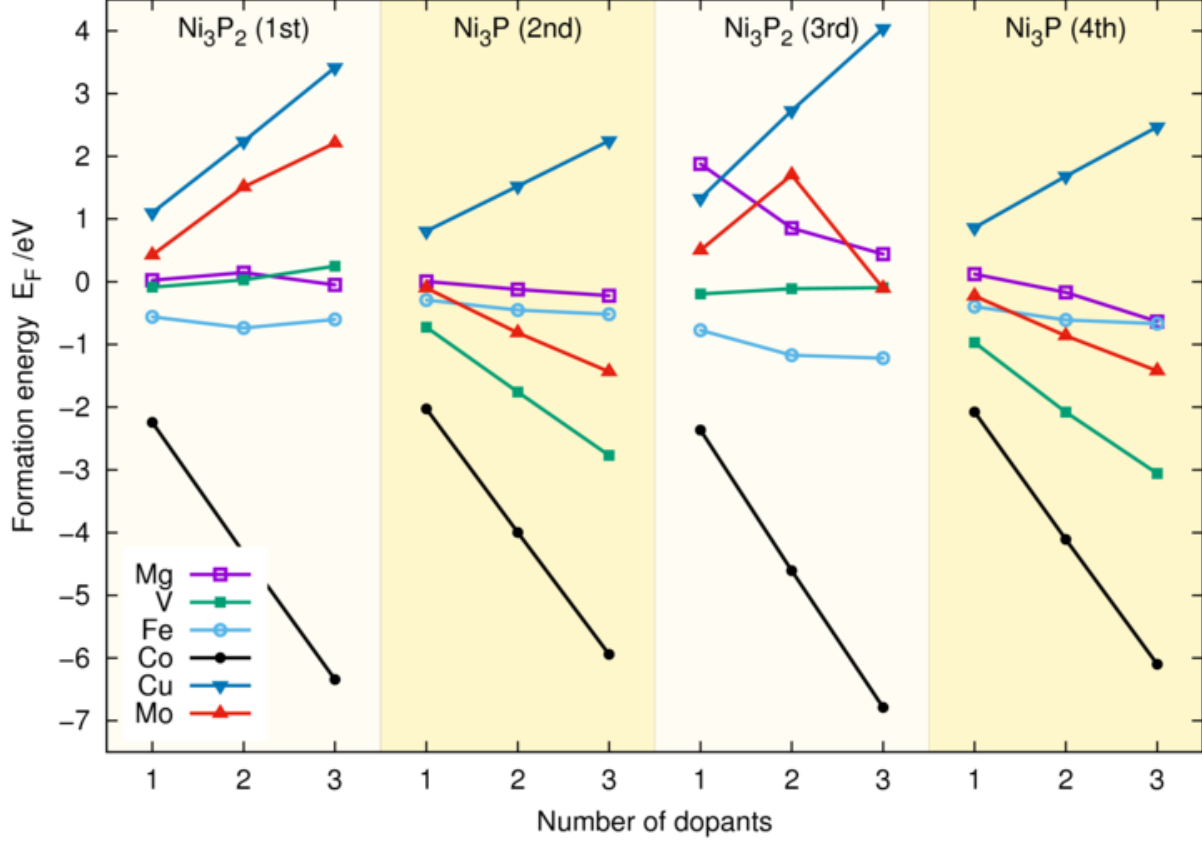

Figure 4: Doping energies (E_F) for Mg, V, Fe, Co, Cu, and Mo for the four topmost layers of the Ni_3P_2+P termination of Ni_2P.

3.2 Hydrogen adsorption free energies

Ni_3P_2 termination

The hydrogen adsorption free energies predicted with equation (7) are summarised in Figure 5 for the Ni_3P_2 terminated Ni_2P. The full data is provided in pictorial form in the Supple-

mentary Information. In the calculations, first one hydrogen was placed in one of fourteen random locations above the surface, as described in Section 2.2. The lowest adsorption free energies from these calculations are shown as black triangles in Figure 5, and with the exception of the l2d3-doped Mg, these lie clearly below the optimal range of ±0.1 eV.

Aligned with previous studies on pristine and Al-doped Ni_3P_2 surfaces,[26,28,54] we find a strongly binding Ni_3-hollow site together with a number of more weakly binding sites. In most studied surfaces, the first hydrogen is found in the Ni_3 deep site with the exception of Mg where it is located on the Ni-Ni bridge of the Ni_3 site. In these three bridge configurations, the closer the hydrogen is to the centre of the Ni_3 site (or in the case of Mg (l1d1) the Ni_2Mg site) the lower the ΔG_H-value. In addition to the Mg-doped cases, also the l1d2 Co doping had the hydrogen localise to a Co-Co bridge site for the lowest free energy configuration. As the H also moved towards the Ni-atoms from the centre of the Ni_3 site for the l1d1 doping with Cu and Mo, we conclude that the prevalent adsorption pattern of H on the strongly binding Ni_3 hollow site is most perturbed by substitutional doping of the first layer, at least in low doping conditions. This is in agreement with the results of Hakala and Laasonen who observed that low Al doping of the surface layer effectively weakened the hollow site's binding energy, resulting in H coordination by just two Ni atoms.[26]

Recently, Wexler et al.[55] were able to show that the effect of nonmetal surface doping of the P atoms surrounding the Ni_3 site on a Ni_3P_2 surface can be explained through a chemical pressure-like effect.[56] Consequently, the hollow site Ni-Ni bond length works as a good predictor of the ΔG_H value. We also looked at the correlation between these two quantities, but it was not significant in our data, likely because the electronic character of the dopants is more significant at least in the first layer, where the Ni atoms of the hollow site are directly substituted.

The coloured squares in Figure 5 represent the best, i.e., closest to zero ΔG_H values for the second hydrogen adsorption with the H-atom corresponding to the lowest adsorption free energy already on the surface. The colour indicates the number of geometrically different

12
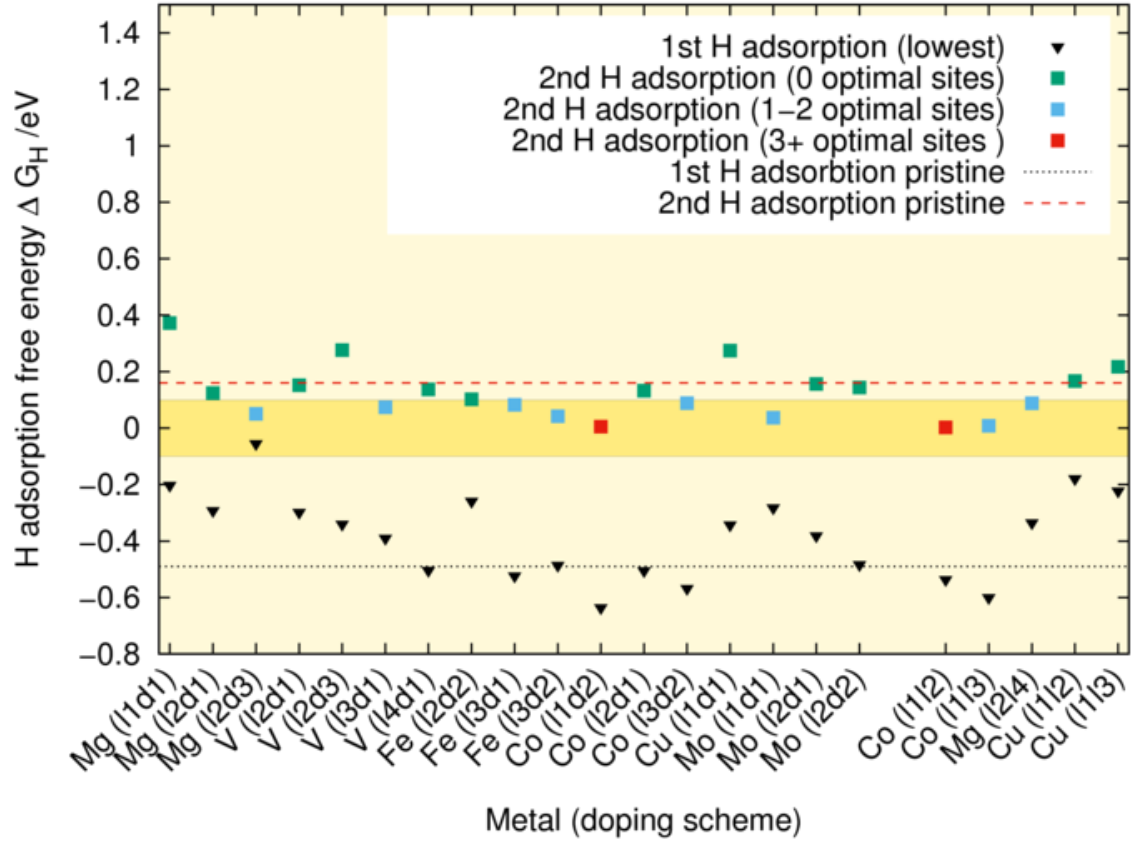
Figure 5: Hydrogen adsorption free energies (ΔG_{H}) for Mg-, V-, Fe-, Co-, Cu-, and Mo-doped Ni_3P_2 terminated Ni_2P. The triangles indicate ΔG_{H} values for the first hydrogen adsorption, whereas the squares signify ΔG_{H} values for the second hydrogen adsorption. The deep yellow band highlights the ± 0.1 eV region around the optimal $\Delta G_{\text{H}} = 0$ value.

sites that fall into the ideal ΔG_H-region. We see that for the Ni_3P_2 termination, Fe and Co doping seems to be particularly effective with plenty of sites in the optimal region for the tested doping schemes. These findings agree with the experimental results on the activating effects of Fe doping.[23,24] In concordance with the predictions of the doping energies of Figure 3, Cu seems to be rather ineffective as a catalyst while the rest of the studied dopants fall somewhere in between. Looking at the V (l4d1) and Mg (l2l4) cases, one sees that inserting dopants to the fourth layer has minimal impact on the adsorption energies. Unsurprisingly, the doping effects on the adsorption free energies generally increase when one moves from the third layer to the second and first ones.

As for the first hydrogen, a number of different adsorption patterns were observed for the second hydrogen. In most cases, the initial hydrogen occupied the hollow Ni_3 site whereas the second hydrogen was located on a nearby Ni-P bridge site. This bonding pattern agrees with the findings of Liu and Rodriguez[54] for the pristine surface. For Mo- and Mg-doped materials showing ideal sites, both hydrogens were located on bridges. In the l1d2-doped Co, we also encountered an energetically favourable configuration where a hydrogen molecule was formed on top of one of the surface Co atoms. The different bonding patterns are illustrated in Figure 6 for Co (l1d2).

Because Hakala and Laasonen[26] found that increasing the supercell surface area did not impact the H-adsorption energies, its effect was not investigated in this study. They also tested how changing the PBE functional to RPBE[57] and turning off the van der Waals interaction affected the ΔG_H values, and found that while the RPBE slightly weakened H binding, the effect of the van der Waals correction was minuscule.[26]

Ni_3P_2+P termination

Analogously to Figure 5, the ΔG_H values for the Ni_3P_2+P terminated Ni_2P are summarised in Figure 7. In addition to the first and second hydrogen adsorptions depicted by triangles and squares, respectively, for calculations where the second hydrogen adsorption energy was
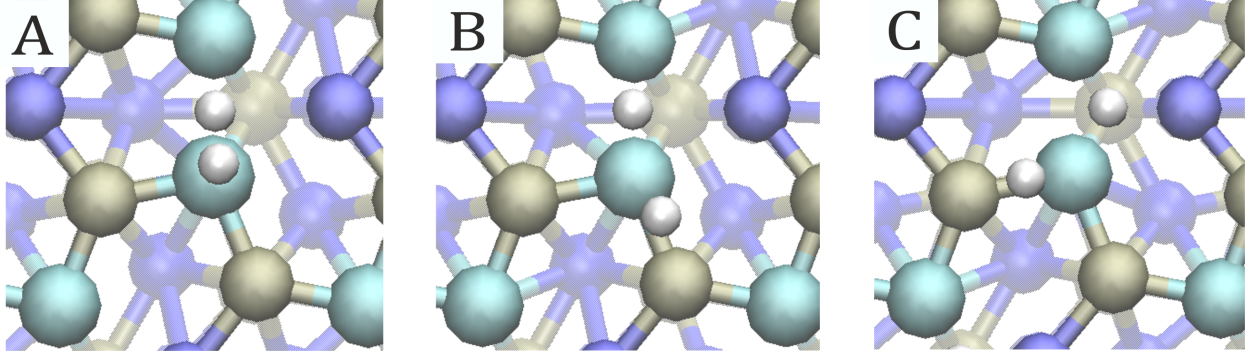
Figure 6: Sample hydrogen adsorption patterns observed in the Co (11d2) surface: A) H_2 formation, B) Co-Co and Co-P bridge site hydrogens, and C) Co_2Ni hollow site and Co-P bridge site hydrogens.

lower than or very similar to the first ΔG_H, free energy values for a third hydrogen adsorption were also calculated. These calculations are indicated by circles and are in all cases with the exception of Fe (11d3) clearly higher in energy than the other two. Again, for the optimal hydrogen adsorption, i.e., the one with ΔG_H values closest to 0, colours are used to indicate the number of distinct adsorption patterns within the optimal energy region. In cases like Co (11d1), where all the first H adsorption free energies are above -0.1 eV and some of the ΔG_H values for the second H adsorption lie within the optimal ± 0.1 range, the coloured symbol is reserved for the adsorption with the larger number of distinct adsorption patterns within the optimal region. As before, it indicates the best free energy value. Finally, the black symbols correspond to the lowest ΔG_H value obtained from the 14 geometry optimisations.

Because the strongly binding Ni_3 site is occupied by the P adatom in Ni_3P_2+P, for some doping schemes in Figure 7, the first hydrogen adsorption already results in the best observed ΔG_H value as indicated by the coloured triangle. Within the accuracy of the DFT calculations, this agrees with the pristine Ni_3P_2+P results indicated by the dashed lines and implies that the surface hydrogen coverage is often lower for this termination.

As expected, doping of the fourth layer in V (14d1) has virtually no effect on the ΔG_H values when compared to the pristine case. Following the trends found in Figure 5, doping of the Ni atoms in layer 3 generally impacts the adsorption free energies less than doping

15
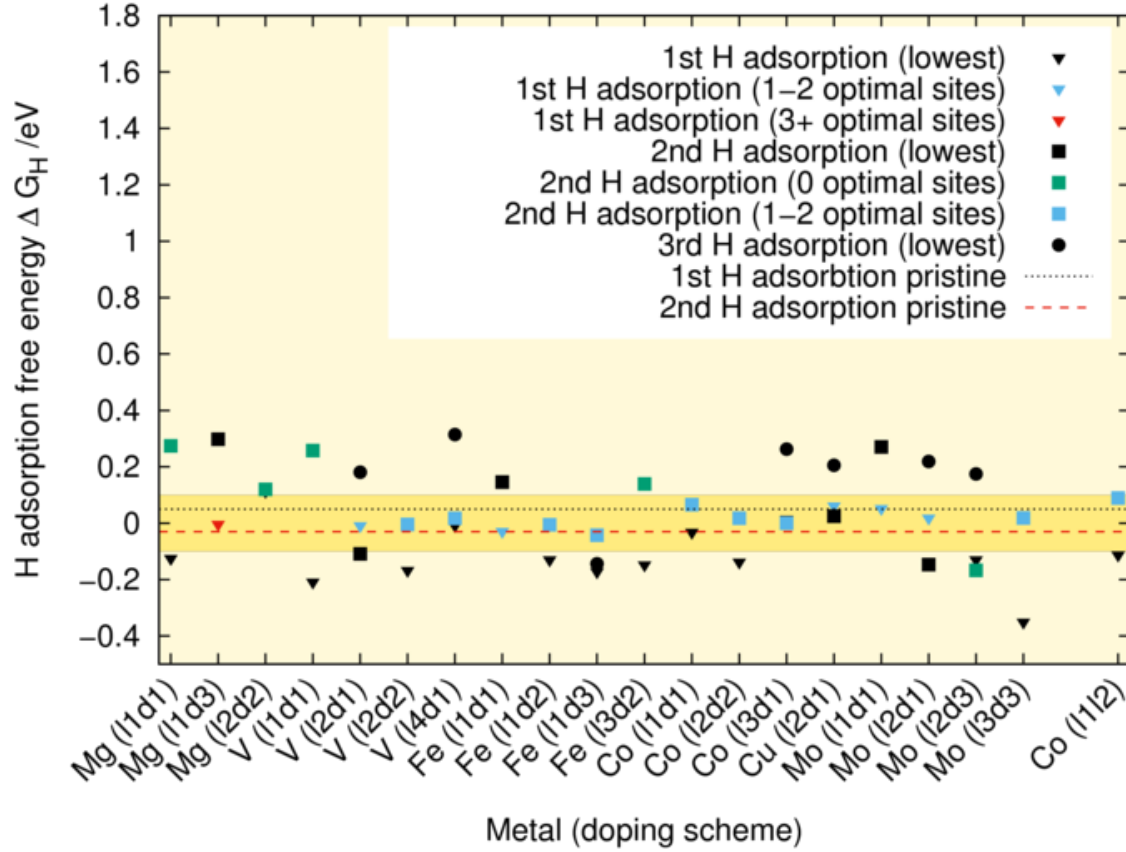
Figure 7: Hydrogen adsorption free energies (ΔG_{H}) for Mg-, V-, Fe-, Co-, Cu-, and Mo-doped Ni_3P_2+P terminated Ni_2P. The triangles indicate ΔG_{H} values for the first hydrogen adsorption, the squares signify ΔG_{H} values for the second hydrogen adsorption, and the circles show ΔG_{H} values for the third hydrogen adsorption. The deep yellow band highlights the ± 0.1 eV region around the optimal $\Delta G_{\mathrm{H}} = 0$ value.

16

at the second or first layers, although the effects become large also at the third layer when the number of dopants increases. Most studied systems in Figure 7 have adsorption energies within the optimal range, indicating that the P adatom leads to surface activation, again in agreement with the pristine case. There does not seem to be a clearly superior candidate for doping material for the Ni_3P_2+P termination. Rather, all the systems function roughly on par with the undoped surface within the optimal region.

In terms of the adsorption geometries for the optimal sites, only the first layer l1d3 Mg doping that is accompanied by a surface reconstruction possesses more than 2 geometrically different active sites for the 1st H adsorption within the energetically optimal region. In most cases, the hydrogen is located on top of the P adatom but in some cases, like V (l2d1) also adsorption on the Ni atoms surrounding the P adatom is observed. With 2 hydrogens adsorbed on the surface, typically at least one of them is located on top of the P adatom. Often, such as in Co (l2d2), both hydrogens are on top of the P adatom, but are oriented in symmetrically non-equivalent directions as illustrated in Figure 8 for Co (l2d2). Similarly to Wexler et al.[28] and Hakala et al.,[26] we find that the P adatom can adsorb up to three hydrogens. However, in all cases where hydrogen adsorption of three hydrogens was considered, spontaneous H_2 formation was also observed during some of the geometry optimisations, underlining the high reactivity of these surfaces.

4 Conclusions

In this study, we have looked at HER on metal-doped Ni_3P_2 and Ni_3P_2+P terminated Ni_2P surfaces. The catalytic HER activity of the studied materials was predicted through DFT calculations by using the hydrogen adsorption free energy as a predictor following the self-consistent scheme proposed by Nørskov et al.[6] and Skúlason et al.[50] Our calculations indicate that doping can substantially improve the catalytic activity of the Ni_3P_2 terminated Ni_2P surface, in agreement with experimental studies. Particularly iron and cobalt emerged as
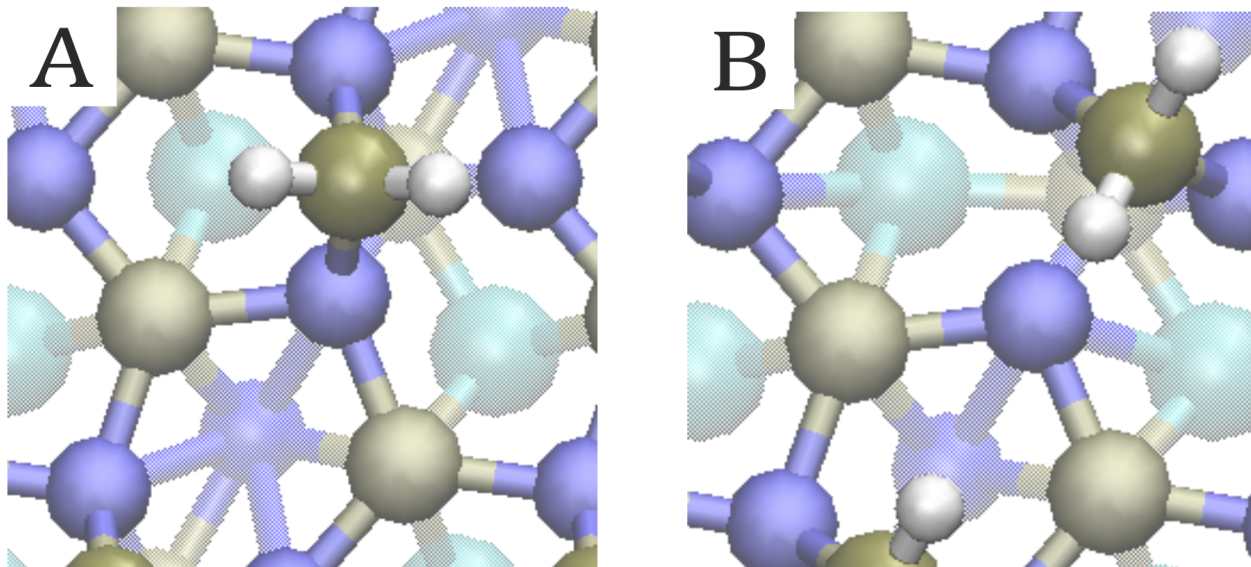
Figure 8: Sample hydrogen adsorption patterns observed in the Co (l2d2) surface: A) Hydrogens on top P adatom and B) Hydrogens on top P adatom with different orientation.

promising dopants. In contrast, the Ni_3P_2+P termination seems to be catalytically active irrespective of the type of doping and even in the absence of doping.

In addition to the ΔG_H values, we also looked at the formation energies of the doped materials to investigate their stability. We predict that the surface should be readily dopable by Co and Fe, for example, whereas for Cu all the energies were unfavourable. Based on our results, the most promising candidates for doping material are iron and cobalt, whereas copper is less likely to function well as a dopant. The rest of the studied metals, V, Mg, and Mo, are predicted to be roughly equal in their applicability.

For the doping geometries, in most cases on Ni_3P_2 the first hydrogen is adsorbed to the strongly binding Ni_3 hollow site, although in some cases it preferred a bridge site on the hollow's edge. In Ni_3P_2+P, the Ni_3 -site is filled by a P adatom. Consequently, for the second hydrogen in the Ni_3P_2 case and the first, second, and third hydrogen adsorptions in the Ni_3P_2+P case, a number of highly active geometrical arrangements were identified with large variations between dopants and doping schemes. In line with previous studies, we find that the P adatom can adsorb up to three hydrogens. However, spontaneous H_2 formation was

18

observed during some of the geometry optimisations in all adsorption calculations involving three hydrogens, which underscores the high reactivity of the Ni_3P_2+P surfaces.

Acknowledgement

References

(1) Lewis, N. S.; Nocera, D. G. Powering the planet: Chemical challenges in solar energy utilization. *Proc. Natl. Acad. Sci. U. S. A.* **2006**, *103*, 15729–15735.

(2) Osterloh, F. E.; Parkinson, B. A. Recent developments in solar water-splitting photocatalysis. *MRS Bull.* **2011**, *36*, 17–22.

(3) Seh, Z. W.; Kibsgaard, J.; Dickens, C. F.; Chorkendorff, I.; Nørskov, J. K.; Jaramillo, T. F. Combining theory and experiment in electrocatalysis: Insights into materials design. *Science* **2017**, *355*, eaad4998(12).

(4) Park, H. G.; Holt, J. K. Recent advances in nanoelectrode architecture for photochemical hydrogen production. *Energy Environ. Sci.* **2010**, *3*, 1028–1036.

(5) Walter, M. G.; Warren, E. L.; McKone, J. R.; Boettcher, S. W.; Mi, Q.; Santori, E. A.; Lewis, N. S. Solar water splitting cells. *Chem. Rev.* **2010**, *110*, 6446–6473.

(6) Nørskov, J. K.; Bligaard, T.; Logadottir, A.; Kitchin, J. R.; Chen, J. G.; Pandelov, S.; Stimming, U. Trends in the exchange current for hydrogen evolution. *J. Electrochem. Soc.* **2005**, *152*, J23–J26.

(7) Wang, Y.; Kong, B.; Zhao, D.; Wang, H.; Selomulya, C. Strategies for developing transition metal phosphides as heterogeneous electrocatalysts for water splitting. *Nano Today* **2017**, *15*, 26 – 55.

(8) Cui, W.; Liu, Q.; Cheng, N.; Asiri, A. M.; Sun, X. Activated carbon nanotubes: a highly-active metal-free electrocatalyst for hydrogen evolution reaction. *Chem. Commun.* **2014**, *50*, 9340–9342.

(9) Davodi, F.; Tavakkoli, M.; Lahtinen, J.; Kallio, T. Straightforward synthesis of nitrogen-doped carbon nanotubes as highly active bifunctional electrocatalysts for full water splitting. *J. Catal.* **2017**, *353*, 19 – 27.

(10) Zheng, Y.; Jiao, Y.; Zhu, Y.; Li, L. H.; Han, Y.; Chen, Y.; Du, A.; Jaroniec, M.; Qiao, S. Z. Hydrogen evolution by a metal-free electrocatalyst. *Nat. Commun.* **2014**, *5*, 3783.

(11) Feng, L.; Xue, H. Advances in transition-metal phosphide applications in electrochemical energy storage and catalysis. *ChemElectroChem* **2017**, *4*, 20–34.

(12) Xiao, P.; Chen, W.; Wang, X. A review of phosphide-based materials for electrocatalytic hydrogen evolution. *Adv. Energy Mater.* **2015**, *5*, 1500985.

(13) Pomerantseva, E.; Resini, C.; Kovnir, K.; Kolen'ko, Y. V. Emerging nanostructured electrode materials for water electrolysis and rechargeable beyond Li-ion batteries. *Adv. Phys.: X* **2017**, *2*, 211–253.

(14) Xie, J.; Zhang, J.; Li, S.; Grote, F.; Zhang, X.; Zhang, H.; Wang, R.; Lei, Y.; Pan, B.; Xie, Y. Controllable disorder engineering in oxygen-incorporated MoS_2 ultrathin nanosheets for efficient hydrogen evolution. *J. Am. Chem. Soc.* **2013**, *135*, 17881–17888.

(15) Xiao, P.; Sk, M. A.; Thia, L.; Ge, X.; Lim, R. J.; Wang, J.-Y.; Lim, K. H.; Wang, X. Molybdenum phosphide as an efficient electrocatalyst for the hydrogen evolution reaction. *Energy Environ. Sci.* **2014**, *7*, 2624–2629.

(16) Popczun, E. J.; McKone, J. R.; Read, C. G.; Biacchi, A. J.; Wiltrout, A. M.; Lewis, N. S.; Schaak, R. E. Nanostructured nickel phosphide as an electrocatalyst for the hydrogen evolution reaction. *J. Am. Chem. Soc.* **2013**, *135*, 9267–9270.

(17) Feng, L.; Vrubel, H.; Bensimon, M.; Hu, X. Easily-prepared dinickel phosphide (Ni_2P) nanoparticles as an efficient and robust electrocatalyst for hydrogen evolution. *Phys. Chem. Chem. Phys.* **2014**, *16*, 5917–5921.

(18) Wang, X.; Kolen'ko, Y. V.; Bao, X.-Q.; Kovnir, K.; Liu, L. One-step synthesis of self-supported nickel phosphide nanosheet array cathodes for efficient electrocatalytic hydrogen generation. *Angew. Chem. Int. Ed.* **2015**, *54*, 8188–8192.

(19) Sun, Y.; Hang, L.; Shen, Q.; Zhang, T.; Li, H.; Zhang, X.; Lyu, X.; Li, Y. Mo doped Ni_2P nanowire arrays: an efficient electrocatalyst for the hydrogen evolution reaction with enhanced activity at all pH values. *Nanoscale* **2017**, *9*, 16674–16679.

(20) Lado, J. L.; Wang, X.; Paz, E.; Carbó-Argibay, E.; Guldris, N.; Rodríguez-Abreu, C.; Liu, L.; Kovnir, K.; Kolen'ko, Y. V. Design and synthesis of highly active Al–Ni–P foam electrode for hydrogen evolution reaction. *ACS Catal.* **2015**, *5*, 6503–6508.

(21) Zhang, Y.; Liu, Y.; Ma, M.; Ren, X.; Liu, Z.; Du, G.; Asiri, A. M.; Sun, X. A Mn-doped Ni_2P nanosheet array: An efficient and durable hydrogen evolution reaction electrocatalyst in alkaline media. *Chem. Commun.* **2017**, *53*, 11048–11051.

(22) Jin, Z.; Li, P.; Huang, X.; Zeng, G.; Jin, Y.; Zheng, B.; Xiao, D. Three-dimensional amorphous tungsten-doped nickel phosphide microsphere as an efficient electrocatalyst for hydrogen evolution. *J. Mater. Chem. A* **2014**, *2*, 18593–18599.

(23) Wang, P.; Pu, Z.; Li, Y.; Wu, L.; Tu, Z.; Jiang, M.; Kou, Z.; Amiinu, I. S.; Mu, S. Iron-doped nickel phosphide nanosheet arrays: An efficient bifunctional electrocatalyst for water splitting. *ACS Appl. Mater. Interfaces* **2017**, *9*, 26001–26007.

(24) Li, Y.; Zhang, H.; Jiang, M.; Zhang, Q.; He, P.; Sun, X. 3D self-supported Fe-doped Ni_2P nanosheet arrays as bifunctional catalysts for overall water splitting. *Adv. Funct. Mater.* **2017**, *27*, 1702513.

(25) Hakala, M.; Kronberg, R.; Laasonen, K. Hydrogen adsorption on doped MoS_2 nanostructures. *Sci. Rep.* **2017**, *7*, 15243.

(26) Hakala, M.; Laasonen, K. Hydrogen adsorption trends on Al-doped Ni_2P surfaces for optimal catalyst design. *Phys. Chem. Chem. Phys.* **2018**, *20*, 13785–13791.

(27) Wexler, R. B.; Martirez, J. M. P.; Rappe, A. M. Stable phosphorus-enriched (0001) surfaces of nickel phosphides. *Chem. Mater.* **2016**, *28*, 5365–5372.

(28) Wexler, R. B.; Martirez, J. M. P.; Rappe, A. M. Active role of phosphorus in the hydrogen evolving activity of nickel phosphide (0001) surfaces. *ACS Catal.* **2017**, *7*, 7718–7725.

(29) Hansen, M. H.; Stern, L.-A.; Feng, L.; Rossmeisl, J.; Hu, X. Widely available active sites on Ni_2P for electrochemical hydrogen evolution – insights from first principles calculations. *Phys. Chem. Chem. Phys.* **2015**, *17*, 10823–10829.

(30) Greeley, J.; Jaramillo, T. F.; Bonde, J.; Chorkendorff, I.; Nørskov, J. K. Computational high-throughput screening of electrocatalytic materials for hydrogen evolution. *Nat. mater.* **2006**, *5*, 909–913.

(31) VandeVondele, J.; Krack, M.; Mohamed, F.; Parrinello, M.; Chassaing, T.; Hutter, J. QUICKSTEP: Fast and accurate density functional calculations using a mixed gaussian and plane waves approach. *Comput. Phys. Commun.* **2005**, *167*, 103–128.

(32) Hutter, J.; Iannuzzi, M.; Schiffmann, F.; VandeVondele, J. cp2k: atomistic simulations of condensed matter systems. *WIREs Comput. Mol. Sci.* **2014**, *4*, 15–25.

(33) Perdew, J. P.; Burke, K.; Ernzerhof, M. Generalized gradient approximation made simple. *Phys. Rev. Lett.* **1996**, *77*, 3865–3868.

(34) Goedecker, S.; Teter, M.; Hutter, J. Separable dual-space Gaussian pseudopotentials. *Phys. Rev. B Condens. Matter* **1996**, *54*, 1703–1710.

(35) Hartwigsen, C.; Goedecker, S.; Hutter, J. Relativistic separable dual-space Gaussian pseudopotentials from H to Rn. *Phys. Rev. B* **1998**, *58*, 3641–3662.

(36) Krack, M. Pseudopotentials for H to Kr optimized for gradient-corrected exchange-correlation functionals. *Theor. Chem. Acc.* **2005**, *114*, 145–152.

(37) Haas, P.; Tran, F.; Blaha, P. Calculation of the lattice constant of solids with semilocal functionals. *Phys. Rev. B* **2009**, *79*, 085104.

(38) Reshak, A. H.; Jamal, M. Calculation of the lattice constant of hexagonal compounds with two dimensional search of equation of state and with semilocal functionals a new package (2D-optimize). *J. Alloy. Compd.* **2013**, *555*, 362 – 366.

(39) Tran, F.; Laskowski, R.; Blaha, P.; Schwarz, K. Performance on molecules, surfaces, and solids of the Wu-Cohen GGA exchange-correlation energy functional. *Phys. Rev. B* **2007**, *75*, 115131.

(40) Wedig, U.; Jansen, M.; Paulus, B.; Rosciszewski, K.; Sony, P. Structural and electronic properties of Mg, Zn, and Cd from Hartree-Fock and density functional calculations including hybrid functionals. *Phys. Rev. B* **2007**, *75*, 205123.

(41) Grimme, S.; Antony, J.; Ehrlich, S.; Krieg, H. A Consistent and accurate ab initio parametrization of density functional dispersion correction (DFT-D) for the 94 elements H-Pu. *J. Chem. Phys.* **2010**, *132*, 154104.

(42) Grimme, S.; Ehrlich, S.; Goerigk, L. Effect of the damping function in dispersion corrected density functional theory. *J. Comput. Chem.* **2011**, *32*, 1456–1465.

(43) Li, Q.; Hu, X. First-principles study of Ni$_2$P (0001) surfaces. *Phys. Rev. B* **2006**, *74*, 035414.

(44) Hernandez, A. B.; Ariga, H.; Takakusagi, S.; Kinoshita, K.; Suzuki, S.; Otani, S.; Oyama, S. T.; Asakura, K. Dynamical LEED analysis of Ni$_2$P (0001)-1×1: Evidence for P-covered surface structure. *Chem. Phys. Lett.* **2011**, *513*, 48 – 52.

(45) Kanama, D.; Oyama, S. T.; Otani, S.; Cox, D. F. Photoemission and LEED characterization of Ni$_2$P(0001). *Surf. Sci.* **2004**, *552*, 8 – 16.

(46) Moula, M. G.; Suzuki, S.; Chun, W.-J.; Otani, S.; Oyama, S. T.; Asakura, K. Surface structures of Ni$_2$P (0001) scanning tunneling microscopy (STM) and low-energy electron diffraction (LEED) characterizations. *Surf. Interface Anal.* **2006**, *38*, 1611–1614.

(47) Suzuki, S.; Moula, G. M.; Miyamoto, T.; Nakagawa, Y.; Kinosthita, K.; Asakura, K.; Oyama, S. T.; Otani, S. Scanning tunneling microscopy and photoemission electron microscopy studies on single crystal Ni$_2$P surfaces. *J. Nanosci. Nanotechno.* **2009**, *9*, 195–201.

(48) Guo, D.; Nakagawa, Y.; Ariga, H.; Suzuki, S.; Kinoshita, K.; Miyamoto, T.; Takakusagi, S.; Asakura, K.; Otani, S.; Oyama, S. T. STM studies on the reconstruction of the Ni$_2$P (10$\bar{1}$0) surface. *Surf. Sci.* **2010**, *604*, 1347 – 1352.

(49) Ariga, H.; Kawashima, M.; Takakusagi, S.; Asakura, K. Density function theoretical investigation on the Ni$_3$PP structure and the hydrogen adsorption property of the Ni$_2$P(0001) surface. *Chem. Lett.* **2013**, *42*, 1481–1483.

(50) Skúlason, E.; Karlberg, G. S.; Rossmeisl, J.; Bligaard, T.; Greeley, J.; Jónsson, H.; Nørskov, J. K. Density functional theory calculations for the hydrogen evolution reac-

tion in an electrochemical double layer on the Pt(111) electrode. *Phys. Chem. Chem. Phys.* **2007**, *9*, 3241–3250.

(51) Nørskov, J. K.; Rossmeisl, J.; Logadottir, A.; Lindqvist, L.; Kitchin, J. R.; Bligaard, T.; Jónsson, H. Origin of the overpotential for oxygen reduction at a fuel-cell cathode. *J. Phys. Chem. B* **2004**, *108*, 17886–17892.

(52) Liu, P.; Rodriguez, J. A.; Asakura, T.; Gomes, J.; Nakamura, K. Desulfurization reactions on $Ni_2P(001)$ and α-$Mo_2C(001)$ surfaces: Complex role of P and C sites. *J. Phys. Chem. B* **2005**, *109*, 4575–4583.

(53) Rodriguez, J. A.; Kim, J.-Y.; Hanson, J. C.; Sawhill, S. J.; Bussell, M. E. Physical and chemical properties of MoP, Ni_2P, and MoNiP hydrodesulfurization catalysts: Time-resolved X-ray diffraction, density functional, and hydrodesulfurization activity studies. *J. Phys. Chem. B* **2003**, *107*, 6276–6285.

(54) Liu, P.; Rodriguez, J. A. Catalysts for hydrogen evolution from the [NiFe] hydrogenase to the $Ni_2P(001)$ surface: The importance of ensemble effect. *J. Am. Chem. Soc.* **2005**, *127*, 14871–14878.

(55) Wexler, R. B.; Martirez, J. M. P.; Rappe, A. M. Chemical pressure-driven enhancement of the hydrogen evolving activity of Ni_2P from nonmetal surface doping interpreted via machine learning. *J. Am. Chem. Soc.* **2018**, *140*, 4678–4683.

(56) Raaen, S.; Parks, R. D. Mixed valence in $CeNi_5$; effects of dilution and chemical pressure. *Solid State Commun.* **1983**, *48*, 199 – 202.

(57) Hammer, B.; Hansen, L. B.; Nørskov, J. K. Improved adsorption energetics within density-functional theory using revised Perdew-Burke-Ernzerhof functionals. *Phys. Rev. B* **1999**, *59*, 7413–7421.